9990–9997 *Nucleic Acids Research, 2019, Vol. 47, No. 19* *Published online 23 September 2019*
doi: 10.1093/nar/gkz812

Interbase FRET in RNA: from A to Z

Anders F. Füchtbauer [1,†], Moa S. Wranne [1,†], Mattias Bood [2,3], Erik Weis [2,3], Pauline Pfeiffer[1], Jesper R. Nilsson [1], Anders Dahlén [3], Morten Grøtli [2] and L. Marcus Wilhelmsson [1,*]

[1]Department of Chemistry and Chemical Engineering, Chalmers University of Technology, Gothenburg SE-412 96, Sweden, [2]Department of Chemistry and Molecular Biology, University of Gothenburg, Gothenburg SE-412 96, Sweden and [3]Medicinal Chemistry, Research and Early Development Cardiovascular, Renal and Metabolism, BioPharmaceuticals R&D, AstraZeneca, Gothenburg, Sweden

Received July 12, 2019; Revised September 02, 2019; Editorial Decision September 09, 2019; Accepted September 11, 2019

ABSTRACT

Interbase FRET can reveal highly detailed information about distance, orientation and dynamics in nucleic acids, complementing the existing structure and dynamics techniques. We here report the first RNA base analogue FRET pair, consisting of the donor tC^O and the non-emissive acceptor tC_{nitro}. The acceptor ribonucleoside is here synthesised and incorporated into RNA for the first time. This FRET pair accurately reports the average structure of A-form RNA, and its utility for probing RNA structural changes is demonstrated by monitoring the transition from A- to Z-form RNA. Finally, the measured FRET data were compared with theoretical FRET patterns obtained from two previously reported Z-RNA PDB structures, to shed new light on this elusive RNA conformation.

INTRODUCTION

The biological roles of the different RNAs are vital and diverse, and include coding, regulation, and expression of genes as well as catalysis. This reflects the importance of secondary and tertiary structure and dynamics for their function, which underlines the need for developing tools that can probe such parameters (1). Förster resonance energy transfer (FRET) is a process in which energy is transferred non-radiatively between a donor and acceptor chromophore. The efficiency of this process is highly dependent on both distance and orientation between the chromophores; hence information about the structure and/or relative position of different donor- and acceptor-labelled biomolecules, under *in vitro* physiological conditions or even in live cells, can be obtained (2,3). FRET is particularly valuable for studying large and flexible structures such as RNAs and RNA–protein complexes that are not easily amenable to traditional high-resolution techniques such as NMR and X-ray crystallography (4). The method can also be used to obtain more detailed structure and dynamics information by, for example, combining single-molecule FRET measurements with detailed analysis and modelling (5).

To date, external chromophores with (supposedly) random orientation have been used for most FRET studies to probe co-localisation and distances, which means that only the distance dependence is used. For example, the ion-induced folding of kink-turns in RNA has been investigated using end-labelling with fluorescein and Cy3 (6). One way to increase the level of information obtained from FRET in RNA systems would be to use fluorescent base analogues, which are firmly positioned inside the nucleic acid and hence report on both the distance and the relative orientation between donor and acceptor. This has been shown to allow structural changes within DNA to be probed with high accuracy (7,8). Until now, a limited number of FBAs have been reported for RNA, e.g. tC^O (9), the thieno[3,4-*d*]pyrimidines (thA, thC, thG and thU) (10) and isothiazolo[4,3-*d*]pyrimidines (^{tz}A, ^{tz}C, ^{tz}G and ^{tz}U) (11), a U surrogate with applications in RNA small molecule binding studies (12), a pyrimidine analogue for G-quadruplex studies (13), and the expanded RNA nucleosides (xRNAs) (14). However, interbase FRET has only been explored for DNA using either a non-emissive acceptor (FRET-pairs tC^O–tC_{nitro} (15), qAN1–qA_{nitro} (8) and pA–qA_{nitro} (16)) or an emissive acceptor (thdG–tC) (17). The use of an emissive acceptor can in theory allow for a simple colorimetric readout and a straightforward and useful internal control of the FRET-efficiency, provided that the emission band of the donor and acceptor are significantly separated. However, most highly emissive FBAs emit within a fairly narrow wavelength region (400–500 nm), and the resulting emission overlap may add an additional layer of complexity and uncertainty to the FRET analysis. In contrast, a non-emissive acceptor allows the FRET efficiency to be quantified simply as the reduction of donor fluorescence (or lifetime) relative

*To whom correspondence should be addressed. Tel: +46 317723051; Email: marcus.wilhelmsson@chalmers.se
†The authors wish it to be known that, in their opinion, the first two authors should be regarded as joint First Authors.

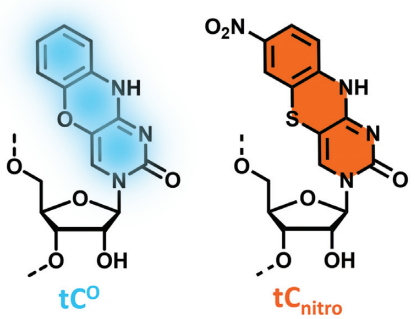

Figure 1. Structure of emissive FRET donor tC^O and non-emissive FRET acceptor tC_{nitro}.

to that of the donor alone, greatly simplifying data analysis and improving accuracy.

Herein, we report on the first interbase FRET investigations in RNA, using the tC^O–tC_{nitro} FRET pair (Figure 1). The non-emissive acceptor molecule, tC_{nitro}, is synthesised and characterised for the first time for use in RNA contexts. In a benchmark study, we see excellent agreement between observed and theoretically predicted FRET efficiency values for A-form RNA, with no significant signs of structural perturbation compared with a natural A-form RNA duplex, indicating that this FRET pair can be used to probe structural changes within RNA with high accuracy. Moreover, the general use of interbase FRET for investigating structural changes in RNA is demonstrated here using the conformational change from A- to Z-form.

MATERIALS AND METHODS

The synthesis and characterisation of the ribo-tC_{nitro} phosphoramidite are provided in the Supplementary Data. The ribo-tC^O phosphoramidite was synthesised according to the literature (9). The solid-phase synthesis of tC^O/tC_{nitro}-modified oligoribonucleotides and their characterisation are described in the Supplementary Data.

All samples used, unless stated otherwise, were prepared in a 10 mM sodium phosphate buffer, pH 7.4 with 100 mM added NaCl and 1 mM EDTA. All samples were mixed and handled in sterile, RNase-free environments. The oligonucleotide concentration was determined by measuring the absorption at 260 nm. The molar absorptivities of the unmodified oligonucleotide single strands at 260 nm were calculated using IDT's online oligonucleotide analyser (Integrated DNA Technologies; http://eu.idtdna.com/calc/analyzer). Molar absorptivities of modified strands were calculated in the same way, with the modified base replaced by cytosine, and correcting for the molar absorptivity difference between cytosine ($\varepsilon = 7400\ M^{-1}\ cm^{-1}$) and tC^O ($\varepsilon = 11000\ M^{-1}\ cm^{-1}$) or tC_{nitro} ($\varepsilon = 9700\ M^{-1}\ cm^{-1}$) at 260 nm.

Hybridisation of A-form RNA samples used for UV-melting and circular dichroism was achieved by mixing each donor strand with an equal amount of acceptor strand at 22°C, followed by rapid heating to 95°C and, after 10 min, cooling to 5°C at 7.5°C h^{-1}. The donor strand concentration during annealing was 4 μM. The A–Z form RNA samples used for UV-melting and circular dichroism were prepared in a similar manner, except that each donor strand was mixed with 30% excess of its complimentary strand (to ensure full hybridisation of the donor strands) and that the donor concentration during annealing was 5.08 μM.

Samples for the A-RNA FRET benchmark study were hybridised as above with 30% excess of its complementary strand (to ensure full hybridisation of the donor strands) and a donor strand concentration of 2 μM during annealing.

Hybridisation of samples for the A- to Z-RNA FRET study was achieved by mixing each donor strand with 100% excess of its complementary strand at 22°C, followed by rapid heating to 75°C and, after 10 min, cooling to 55°C at 1.7°C h^{-1}, followed by cooling to 5°C at 60°C h^{-1}. The donor strand concentration during annealing was 20 μM (a higher concentration was chosen to promote hetero-duplex annealing over self-annealing into hairpins).

All samples used for measuring A-form RNA were subsequently diluted to 2 μM with phosphate buffer, whereas Z-form samples were diluted with phosphate buffer and enough $NaClO_4 \cdot H_2O$ (Sigma-Aldrich) to result in the desired $NaClO_4$-concentration (8 M, unless otherwise stated), while taking the resulting change in solution density into account (18), as well as adjusting for differences in sample concentration (determined by the absorption at 260 nm).

All samples were measured immediately after annealing or stored at −20°C between measurements.

RNA UV-melting and circular dichroism

RNA UV-melting curves were recorded on a Cary 4000 (Varian Technologies) with a programmable multi-cell temperature block, by heating from 20°C to 90°C and subsequent cooling to 20°C at a rate of 0.5°C min^{-1}. The absorption at 260 nm was recorded every 0.5°C for two cycles. The duplex concentration was 2 μM in all measurements. The melting temperatures were calculated as the maximum of the first derivative of the UV-melting curves after FFT-filtered smoothing.

Circular dichroism (CD) spectra were recorded on a Chirascan CD spectrometer (Applied Photophysics) scanning between 200 and 600 nm, using an integration time of 0.5 s and three repetitions. The duplex concentration was 2 μM and all spectra were corrected for background contribution.

Fluorescence measurements

Steady-state emission spectra were recorded on a SPEX Fluorolog 3 (Jobin Yvon Horiba) with an excitation wavelength of 377 nm. The duplex concentration of all samples was 2 μM in steady-state and lifetime measurements. Emission was recorded between 385 and 745 nm at a scan rate of 600 nm min^{-1}.

Quantum yields were measured for duplexes with only tC^O present (i.e. no tC_{nitro}) with an excitation wavelength of 356 nm, using quinine sulfate ($\Phi_f = 54.6\%$) in 0.5 M H_2SO_4 as reference. Emission was recorded between 360 and 690 nm at a scan rate of 600 nm min^{-1}.

Fluorescence lifetimes were determined using time-correlated single-photon counting (TCSPC). The samples were excited by a PicoQuant pulsed (10 MHz) laser diode

emitting at 377 nm and the emission monochromator was set to 460 nm. The counts were collected by a R3809U-50 microchannel-plate photomultiplier tube (Hamamatsu) and fed into a Lifespec multi-channel analyser (Edinburgh Analytical Instruments) with 2048 channels. The stop condition was set to 10 000 counts in the top channel. Reconvolutional fitting to bi- or triexponential functions was performed using Fluofit Pro v.4 software (PicoQuant GmbH). The average lifetimes were amplitude weighted according to Equation (1):

$$\langle \tau \rangle = \frac{\sum_i \alpha_i \tau_i}{\sum_i \alpha_i} \quad (1)$$

where $\langle \tau \rangle$ is the average lifetime, τ_i is the ith lifetime and α_i is the amplitude of the ith lifetime. Measurements were duplicated.

The FRET efficiencies were calculated from steady-state emission and fluorescence lifetimes according to Equations (2 and 3):

$$E = 1 - \frac{I_{DA}}{I_D} \quad (2)$$

$$E = 1 - \frac{\tau_{DA}}{\tau_D} \quad (3)$$

where I is the integrated intensity of the donor and τ is the average lifetime of the donor. The subscripts D and DA refers to samples with only donor and with donor and acceptor, respectively.

Theoretical FRET calculations

The Förster distance R_0 (in Å) and the theoretical FRET efficiencies E were calculated according to the following equations:

$$R_0 = 0.211\left(\kappa^2 \eta^{-4} \Phi_D J(\lambda)\right)^{1/6} \quad (4)$$

$$E = \frac{R_0^6}{R_0^6 + {R_{DA}}^6} \quad (5)$$

where η is the refractive index of the medium (1.4 for biomolecules), Φ_D is the quantum yield of the donor, $J(\lambda)$ is the overlap integral, R_{DA} is the distance between donor and acceptor, and κ^2 is an orientation factor describing the relative orientation of the donor and acceptor transition dipole moments. With knowledge about the photophysical properties of the FRET pair (Φ_D and $J(\lambda)$) and the relative position and orientation of the donor and acceptor (R_{DA} and κ^2), the expected transfer efficiency was calculated using the MATLAB-based software FRETmatrix (19). The protocol differed slightly for A- and Z-form RNA (Figure 2A) as described below.

A-form. The average base step parameters for A-form were taken from Olson *et al.* (21) Figure 2B shows the six different base step parameters that are used to build models of nucleic acids. To create a smooth curve that guides the eye, each base-step was divided into 10 equally sized steps for which a hypothetical FRET value was calculated. The calculations utilised the orientation of the transition dipole moments of tC^O and tC_{nitro} (22,23), and the experimentally observed quantum yield of tC^O in each sequence context: 19.1% for the A-RNA benchmark study and 20.9% for the A- to Z-RNA study (Supplementary Tables S4 and S8). Using Equation (6), the overlap integral, J_{DA}, was determined experimentally to be 1.7×10^{14} nm^4 M^{-1} cm^{-1} for the A-RNA benchmark study and 1.5×10^{14} nm^4 M^{-1} cm^{-1} for A-form RNA in the A- to Z-RNA study.

$$J_{DA} = \int I_D(\lambda)\, \varepsilon_A(\lambda)\, \lambda^4 d\lambda \quad (6)$$

where I_D is the wavelength-dependent donor emission spectrum normalised to integrate to unity, ε_A is the wavelength-dependent molar absorptivity of the acceptor, and λ is the wavelength in nm.

Z-form. To enable comparison between the three previously reported Z-form structures (1T4X, 2GBX and 1QBJ), which are 6mers, and our structure, which is a 14mer, we utilised a method in which we extend the 6mers of the previously reported PDB-files to 14mers using averaged base-step parameters. The PDB-files were first analysed with Web 3DNA to retrieve the base-step parameters for each structure (24). Each parameter was averaged to create structure-specific averaged GC and CG base-step parameters. Using these parameters, a new base-step file was created for each structure, containing 14, instead of the original 6, base pairs. Finally, using these base-step files, standard Watson-Crick base-pairing geometries, the quantum yield of tC^O in Z-RNA ($\Phi_f = 21.3\%$), and the spectral overlap between tC^O emission and tC_{nitro} absorption in Z-RNA ($J_{DA} = 1.4 \times 10^{14}$ nm^4 M^{-1} cm^{-1}), a theoretical FRET efficiency at different separations for each structure were calculated using FRETmatrix (19).

RESULTS AND DISCUSSION

Synthesis of tC_{nitro}

We recently reported the synthesis and RNA incorporation of the tC^O-ribonucleoside and concluded that ribo-tC^O preserves the A-form duplex, maintains a high quantum yield irrespective of sequence context and, hence, is an excellent FRET donor candidate for interbase FRET in RNA (9). In this study, we report the synthesis of the non-emissive FRET acceptor tC_{nitro}-ribonucleoside and its phosphoramidite substrate **5** (Scheme 1). The 2′-O-TBS-protected ribonucleoside of tC_{nitro} (**4**, Scheme 1) was synthesised on a multigram scale in a five-step protocol. The silyl protecting group of compound **1**, including the 2′-OH TBS protection required for the final building block, was introduced in the first step based on a previously published methodology (25). Compound **1** was then subjected to a Cu-catalysed C-S cross-coupling with thiol **2,** which enabled the selective formation of the C-S bond while preserving the protecting groups and the stereochemistry of the nucleoside moiety, providing compound **3** in 81% yield. The tricyclic aromatic system of tC_{nitro} was constructed with a ring-closing condensation, for which PyBOP proved to be uniquely active. Under mild conditions, the product of the intramolecular condensation was obtained with high selectivity over the intermolecular reaction. The resulting fully

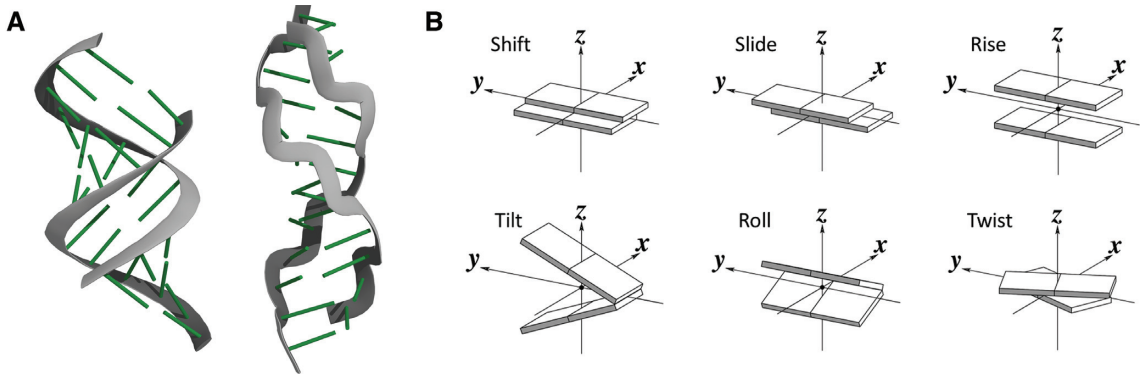

Figure 2. (**A**) General 3D structures of A- and Z-form RNA. (**B**) Illustration of the six base step parameters used when building nucleic acid structures. Figure adapted from Lu *et al.* (20).

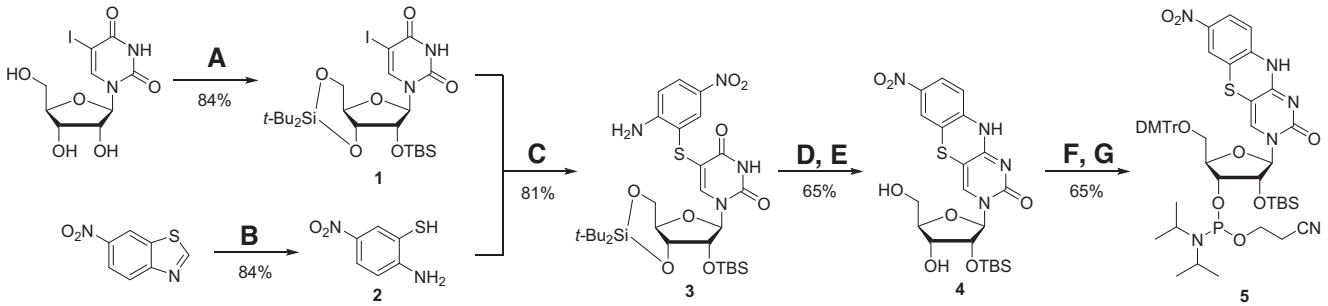

Scheme 1. Synthesis of the tC_{nitro} phosphoramidite **5**. Reagents and conditions: (**A**) *t*-$Bu_2Si(OTf)_2$, DMF, 0°C, 1 h; then imidazole, 0°C, 30 min; then TBS-Cl, RT, 12 h. (**B**) NH_2NH_2(aq.), EtOH, RT, 18 h. (**C**) CuI, Cs_2CO_3, DMSO, 60°C, 24 h. (**D**) PyBOP, DBU, MeCN, 0°C, 1 h; then RT, 4 h. (**E**) Py·$(HF)_x$, CH_2Cl_2, 0°C –> RT, 6 h. (**F**) DMTr-Cl, Py, 0°C, 30 min; then RT, 4 h. (**G**) CEP-Cl, DIPEA, THF, RT, 20 h.

protected tC_{nitro} ribonucleoside was subsequently deprotected to afford compound **4**. Two standard protection steps (26,27), gave the desired tC_{nitro}-phosphoramidite building block **5** for oligoribonucleotide incorporation.

A-form RNA FRET benchmark

To study FRET in RNA using tC^O and tC_{nitro}, we synthesised three donor sequences containing tC^O and four complementary acceptor sequences containing tC_{nitro} (Figure 3A), as well as their unmodified counterparts, termed D0 and A0, respectively. These strands allow the formation of duplexes with 2–13 bp separating the donor and acceptor. The CD spectra of tC_{nitro}-modified duplexes are very similar to that of the corresponding unmodified duplex, indicating that tC_{nitro} does not perturb the A-form (Supplementary Figure S1). Furthermore, the UV-melting properties of tC_{nitro}-modified duplexes indicate that tC_{nitro}, like tC^O, has a slightly stabilising effect on A-form RNA, with the degree of stabilisation depending on nearest neighbors (1.4–1.7°C for 5′-C**tC_{nitro}**U-3′; 3.9–4.2°C for 5′-U**tC_{nitro}**C-3′; Supplementary Table S1) (9).

The fluorescence properties of tC^O and tC_{nitro} in A-form RNA are summarised in Table 1. Importantly, tC^O retains a high and stable fluorescence quantum yield regardless of sequence context (9), and there is an excellent overlap between the long-wavelength emission band of tC^O with the absorption band of tC_{nitro} (Figure 4). Assuming free rotation of the transition dipole moments ($\kappa^2 = 2/3$), the theoretical Förster distance for the tC^O–tC_{nitro} FRET-pair in RNA is 28 Å, corresponding to almost one complete turn of the A-form RNA helix.

A A-form FRET benchmark

```
                D6   D8   D10
5′ CGA CAC ACA CAA GGA CGA GGA UUC C 3′
3′ GCU GUG UGU GUU CCU GCU CCU AAG G 5′
                   A13 A12  A7 A6
```

B A- to Z-form FRET

```
                 D2  D4  A6  A8 A10 A12
5′ CCAACCAA_GCGCGCGCGCGCGC_AACCAACC 3′
3′ GGUUGGUU_CGCGCGCGCGCGCG_UUGGUUGG 5′
                        A9   A13
```

Figure 3. (**A**) RNA sequences used to investigate the interbase FRET characteristics in A-form RNA. (**B**) RNA sequences used for investigating the transition from A- to Z-form RNA. The DX and AY notation of sequences reflects positions of the donor, tC^O (blue), and non-emissive acceptor, tC_{nitro} (orange), in the sequence, counting from (**A**) the 5′-end or (**B**) the 5′-end of the GC-repeat of the donor-containing sequence. Each sequence combination contained only one donor and a maximum of one acceptor. Abasic sites are denoted with an underscore. For a complete listing of all duplexes used for this study, see Supplementary Tables S1 and S7.

To investigate the applicability of interbase FRET using tC^O and tC_{nitro} in RNA systems, the measured FRET efficiency was compared with a theoretical value for A-form RNA, which was calculated from established RNA structure and probe properties. For comparison the theoretical

Table 1. The absorptive and fluorescence properties of tC^O and tC_{nitro} inside double-stranded A-form RNA

	$\lambda_{abs,max}$ [nm]	ε_{max} [M^{-1} cm^{-1}]	$\lambda_{em,max}$ [nm]	Φ_f [%]	$\langle\tau\rangle$ [ns]
tC^O [a]	368–373 (370)	7400–9700 (8300)	452–460 (456)	20–25 (22)	3.8–4.7 (4.3)
tC_{nitro} [b]	449–458 (454)	6400–7100 (6800)	–	–	

[a]Values based on sequences reported by Füchtbauer *et al.* (9) with average values shown in parenthesis.
[b]Values based on RNA duplexes D0A6, D0A7, D0A12 and D0A13 (this work).

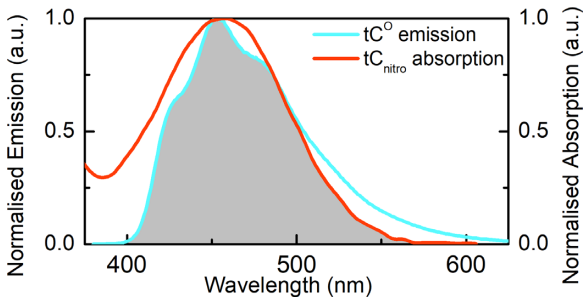

Figure 4. Spectral overlap between tC^O emission and tC_{nitro} absorption in A-form RNA. The spectra are normalised at their long-wavelength maxima. Measurements were performed at RT in phosphate buffer, pH 7.4, 123 mM Na^+.

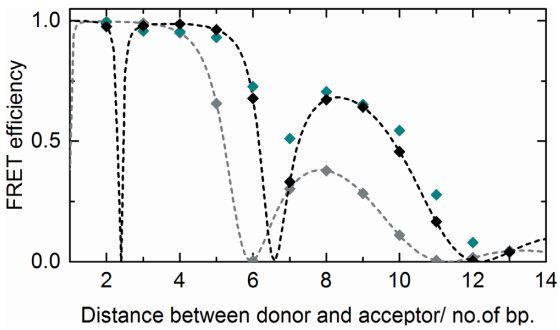

Figure 5. FRET efficiency between tC^O and tC_{nitro} in A-form RNA as a function of base-pair separation. Cyan diamonds mark averaged data from steady-state and lifetime measurements. Black diamonds mark the predicted FRET efficiency for tC^O–tC_{nitro} inside A-form RNA, with a dashed curve showing the predicted FRET efficiency at non-integer separations. Gray diamonds mark the predicted FRET efficiency for tC^O–tC_{nitro} inside B-form nucleic acid, with a dashed curve showing the predicted FRET efficiency at non-integer separations. Measurements were performed at RT in phosphate buffer, pH 7.4, 123 mM Na^+.

values based on B-form RNA were also calculated. In this study, the FRET efficiency as a function of donor-acceptor distance was measured using both steady-state emission and fluorescence lifetime measurements of tC^O in duplexes with and without tC_{nitro} (Supplementary Tables S2 and S3; Supplementary Figure S2). Figure 5 shows the average transfer efficiency from these two methods together with the theoretical FRET efficiency for tC^O–tC_{nitro} inside static A-form and B-form nucleic acid. The dashed curves, showing the transfer efficiency also at unnatural non-integer separations, is added to the figure to guide the eye. The local minima of these curves originate from separations where donor and acceptor transition dipoles would be perpendicular to each other and hence constitute geometries where no energy transfer can take place in this static theoretical representation of the nucleic acid structure.

The measured data follow the predicted A-form FRET pattern closely, showing that the base analogues are firmly stacked inside RNA and strongly suggesting that they do not significantly perturb the RNA structure. Hence, this benchmark study shows that the tC^O–tC_{nitro} FRET pair is excellent for interbase FRET measurements in RNA, especially at separations of 4–12 bp. We have previously shown how the binding of netropsin to DNA and the B- to Z-transition in DNA can be studied using interbase FRET (7,8). Because the photophysical properties of tC^O and tC_{nitro} are well established (see Table 1 above), similar studies inside RNA should now be possible, making interbase FRET using tC^O–tC_{nitro} a powerful complement to existing techniques for studying RNA structure, conformational changes, and dynamics.

A- to Z-form FRET

To illustrate the potential of this method, we designed a study where tC^O–tC_{nitro} interbase FRET was applied to investigate a conformational change in RNA, in this case the A- to Z-RNA transition. The structure of the right-handed B-form DNA and A-form RNA are both well characterised. However, both DNA and RNA can also adopt a left-handed structure termed the Z-form. Z-form DNA was crystallised and characterised using X-ray crystallography for the first time in 1979 (28), whereas the first left-handed structure of RNA was described in 1984 (29). As is the case for Z-form DNA, the transition from A- to Z-form RNA occurs preferentially in alternating GC-repeats but more extreme salt conditions are needed to induce the transformation. The biological role of Z-form RNA is still unclear, but staining with Z-RNA antibodies indicates its presence in the cytoplasm and the nucleolus (30), and certain interferon response proteins have domains that can stabilise Z-form RNA (31). However, there is a lack of tools that can monitor the Z-RNA structural change in live cell systems, and structural studies on Z-RNA are scarce; only two 6mer structures have been submitted to the PDB database: An NMR investigation where the Z-form is induced by high salt concentration (6 M $NaClO_4$, PDB ID: 1T4X) and a crystallographic study of Z-form RNA together with the enzyme ADAR1 (PDB ID: 2GXB) (31,32).

To enable comparison between the structures deposited in the PDB and those used in this study, we applied FRET theory to predict the FRET patterns expected from tC^O–tC_{nitro} when inserted at different positions in two oligoribonucleotides, each with a structure matching one of the PDB entries mentioned above (Figure 6A). Since some studies indicate strong similarities between the DNA and

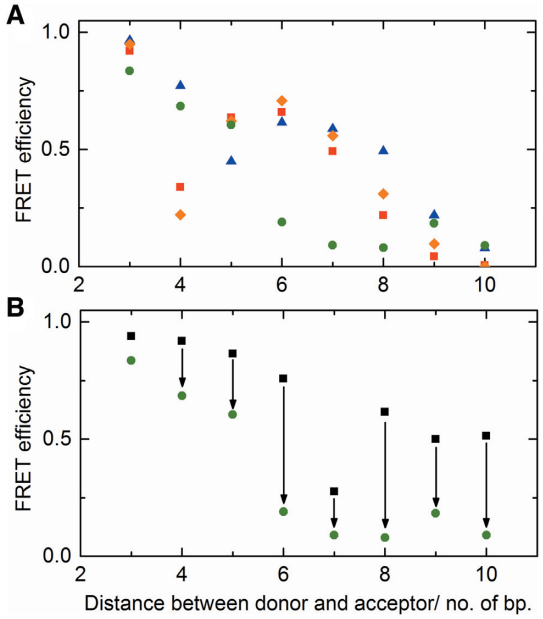

Figure 6. (**A**) Measured FRET efficiency between tC^O and tC_{nitro} for the GC-repeat in Z-form (green circles), together with predicted FRET values of previously reported Z-form structures: PDB entries 1T4X (blue triangles, NMR structure of Z-form RNA in 6 M $NaClO_4$), 2GXB (orange diamonds, crystal structure of Z-form RNA bound to ADAR1) and 1QBJ (red squares, crystal structure of Z-form DNA bound to ADAR1) (31–33). (**B**) Measured FRET efficiency between tC^O and tC_{nitro} for the GC-repeat in A-form (black squares) and Z-form (green circles). Arrows indicate the direction of change upon switching from A- to Z-form. Measurements were performed at RT in phosphate buffer, pH 7.4, 123 mM Na^+ (A-form) or with 8 M $NaClO_4$ added (Z-form), and are averaged data from steady-state and lifetime measurements.

RNA Z-form, the theoretical FRET pattern obtained using the structure of Z-form DNA bound to ADAR1 (PDB ID: 1QBJ) was included as an additional comparison (31,33). As can be seen in Figure 6A, the theoretical FRET pattern for the three reported structures display overall similarities but also significant differences due to the structural variation between them. Because the Z-form primarily occurs in GC-repeats, our cytosine analogues provide an excellent opportunity to study the conformational change from A- to Z-form RNA. Our aim with this A- to Z-form RNA study was twofold: First, to establish if interbase FRET can be used to probe the RNA A- to Z-transition. This conformational change is normally monitored using CD, which requires instrumentation that is less common in R&D labs, considerably higher sample amounts than fluorescence measurements, and is not compatible with measurements *in cellulo*. Second, to obtain novel structural information about Z-RNA and place it in the context of previously determined Z-RNA structures.

Sequences with GC-repeats are very prone to self-dimerisation and hairpin formation, and therefore require a different and more thorough sequence design compared with our initial benchmark study (Figure 3A). To reduce interference from hairpin formation, the GC-repeat was kept as short as possible (14mer) while still allowing for investigation of a complete helix turn, i.e. donor–acceptor separations of up to 10 bp, without end-fraying. Furthermore, the GC-repeat is flanked by one abasic site and eight bases on each side. The eight flanking bases were introduced to keep the ends together in the A-form throughout the experiment, and to increase the stability of the in-frame matched duplex, whereas the abasic sites serve as a flexible linker to allow the GC-repeat to form Z-RNA while the ends remain in A-form.

For this study, 8 M $NaClO_4$ was used to induce the Z-form. CD investigations indicate that the Z-form is stable at room temperature for >18 h under these conditions and that the donor and acceptor do not hinder its formation (Supplementary Figure S3), a further indication that the modified RNA bases serve as good analogues of their natural cytosine counterparts. To investigate the difference between FRET in A- and Z-form RNA, measurements using both steady-state emission and fluorescence lifetimes were performed on both conformations (Figure 6B, Supplementary Figure S4, and Supplementary Tables S5 and S6). Because the donor and acceptor in the GC sequences are in the same strand for odd separations and in opposite strands for even separations, the FRET pattern of the GC-repeat in A-form is different from that of the benchmark study where donor and acceptor are in opposite strands for all separations (Supplementary Figure S5). In the Z-form data there is a discrepancy between steady-state- and lifetime-based FRET efficiencies for separations seven and nine (Supplementary Table S7). These two separations were measured using same-strand labelled sequences where hairpin formation would bring the donor and acceptor very close in space (0–2 bp). At such short distances, donor quenching may be of direct-contact character (e.g. Dexter electron transfer), and therefore occur on a timescale that is unresolvable using our fluorescence lifetime setup. Under such circumstances, only the lifetime of the correctly folded fraction of the sample, i.e. Z-form RNA duplexes, would be visible in the fluorescence decay, while the steady-state emission would be further quenched and therefore give rise to a seemingly higher FRET value. Because our results show a difference between steady-state and lifetime FRET at separation seven and nine and therefore indicate partial formation of 'dark species' (e.g. hairpins) in these samples, only the lifetime-based FRET efficiencies were used for these data points in the subsequent evaluation (Figure 6).

First, we investigated whether RNA interbase FRET could be used to probe the RNA A- to Z-transition. The difference in FRET pattern between A- and Z-form RNA is striking, with 25%-87% change in transfer efficiency for seven out of eight investigated separations (Figure 6B), indicating that the system is sensitive enough to study the change between A- and Z-form RNA by monitoring the change in FRET at only one or a couple of separations. The quantum yield of tC^O is essentially the same in both conformations (Supplementary Table S8), strongly suggesting that the observed changes in transfer efficiency are due to structural changes in the RNA and not due to variations in the probe microenvironment. Taken together, this shows that RNA interbase FRET between tC^O and tC_{nitro} separated by 4–10 bp can probe the A- to Z-RNA structural change with high sensitivity, which further illustrates the overall adapt-

ability of this method for investigating structural changes in nucleic acids. The significant differences in fluorescence lifetime between the corresponding A- and Z-form RNA duplexes point towards possible fluorescence lifetime imaging microscopy (FLIM) applications in which RNA specifically in Z-form could be monitored in live cell microscopy.

Second, we compared our FRET data with the theoretically obtained FRET pattern from the few existing PDB structures. The FRET pattern we obtained for Z-form RNA fits well with those of the previously reported structures at short and long distances (Figure 6A). However, at intermediate distances (6–8 bp), the observed FRET efficiency is considerably lower than the values calculated based on the reported average parameters of the 6mer PDB structures. One explanation for these discrepancies may be that the Z-RNA structure is different for the previously reported short, and inherently less stable, 6mer RNA compared to our 14mer system, where the ends are kept in place by A-form RNA flanking bases. The 6mer Z-RNA structures determined with NMR or X-ray techniques may also be slightly different from the structure in solution at more physiologically relevant RNA concentrations. Given the severe sparsity of reports containing structural information for Z-form RNA, it is too early to comment extensively on the structural uniformity of this RNA duplex form. This would require a larger set of comparative studies addressing aspects such as oligoribonucleotide length and type of associating protein.

CONCLUSION

We have shown that the tC^O–tC_{nitro} FRET pair is well suited to monitor interbase FRET in RNA duplexes. The probes are firmly positioned inside the RNA and the FRET pattern follows the predicted values for A-RNA closely. We observe a large change in FRET efficiency as Z-RNA is formed from the A-form using a high concentration of $NaClO_4$, which shows that, as in DNA, RNA interbase FRET can be used to probe structural changes under physiological conditions with high sensitivity as well as versatility regarding tC^O–tC_{nitro} spacing. When comparing our measured FRET pattern to the few existing PDB structures of Z-form RNA, we find overall similarities but also significant differences. Differences of similar magnitude can also be found between the PDB structures, implying that more Z-RNA structures need to be investigated to determine whether Z-form RNA has one uniform structure with a unique set of parameters to extract. Considering the higher structural diversity and dynamics of RNA and RNA–protein complexes compared with DNA, this represents a significant step forward, not only for interbase FRET as a general nucleic acid methodology but, importantly, for the rapidly growing field of RNA structure and dynamics investigations in particular and RNA research in general. Unlike most structure and dynamics investigation techniques, interbase FRET can be performed under physiological conditions. Hence, we envisage the main usefulness of this method to be in monitoring RNA structural changes in live cell systems, either alone or in hybrid approaches together with X-ray or NMR, to reveal valuable new information about the main molecules of life, the RNAs.

SUPPLEMENTARY DATA

Supplementary Data are available at NAR Online.

ACKNOWLEDGEMENTS

We thank Afaf H. El-Sagheer and Prof. Tom Brown (University of Oxford, UK) for training A.F.F. and M.B. in RNA purification.

FUNDING

Swedish Foundation for Strategic Research [SSF, IS14-0041, IRC15-0065 to L.M.W., ID14-0036 to M.G.]; Swedish Research Council [VR, 2017-03707 to L.M.W.]. Funding for open access charge: Swedish Research Council [VR, 2017-03707].

Conflict of interest statement. None declared.

REFERENCES

1. Dethoff,E.A., Chugh,J., Mustoe,A.M. and Al-Hashimi,H.M. (2012) Functional complexity and regulation through RNA dynamics. *Nature*, **482**, 322–330.
2. Harpur,A.G., Wouters,F.S. and Bastiaens,P.I.H. (2001) Imaging FRET between spectrally similar GFP molecules in single cells. *Nat. Biotechnol.*, **19**, 167–169.
3. Hillger,F., Hanni,D., Nettels,D., Geister,S., Grandin,M., Textor,M. and Schuler,B. (2008) Probing protein-chaperone interactions with single-molecule fluorescence spectroscopy. *Angew. Chem. Int. Ed.*, **47**, 6184–6188.
4. Gubaev,A. and Klostermeier,D. (2013) In: Klostermeier,D. and Hammann,C. (eds). *RNA Structure and Folding: Biophysical Techniques and Prediction Methods*. De Gruyter, Berlin, pp. 181–214.
5. Peulen,T.O., Opanasyuk,O. and Seidel,C.A.M. (2017) Combining graphical and analytical methods with molecular simulations to analyze Time-Resolved FRET measurements of labeled macromolecules accurately. *J. Phys. Chem. B*, **121**, 8211–8241.
6. McPhee,S.A., Huang,L. and Lilley,D.M. (2014) A critical base pair in k-turns that confers folding characteristics and correlates with biological function. *Nat. Commun.*, **5**, 5127.
7. Dumat,B., Larsen,A.F. and Wilhelmsson,L.M. (2016) Studying Z-DNA and B- to Z-DNA transitions using a cytosine analogue FRET-pair. *Nucleic Acids Res.*, **44**, e101.
8. Wranne,M.S., Füchtbauer,A.F., Dumat,B., Bood,M., El-Sagheer,A.H., Brown,T., Gradén,H., Grøtli,M. and Wilhelmsson,L.M. (2017) Toward complete sequence flexibility of Nucleic Acid base analogue FRET. *J. Am. Chem. Soc.*, **139**, 9271–9280.
9. Füchtbauer,A.F., Preus,S., Börjesson,K., McPhee,S.A., Lilley,D.M.J. and Wilhelmsson,L.M. (2017) Fluorescent RNA cytosine analogue – an internal probe for detailed structure and dynamics investigations. *Sci. Rep.*, **7**, 2393.
10. Shin,D., Sinkeldam,R.W. and Tor,Y. (2011) Emissive RNA alphabet. *J. Am. Chem. Soc.*, **133**, 14912–14915.
11. Rovira,A.R., Fin,A. and Tor,Y. (2015) Chemical mutagenesis of an emissive RNA alphabet. *J. Am. Chem. Soc.*, **137**, 14602–14605.
12. Xie,Y., Dix,A.V. and Tor,Y. (2009) FRET enabled real time detection of RNA-Small molecule binding. *J. Am. Chem. Soc.*, **131**, 17605–17614.
13. Tanpure,A.A. and Srivatsan,S.G. (2015) Conformation-sensitive nucleoside analogues as topology-specific fluorescence turn-on probes for DNA and RNA G-quadruplexes. *Nucleic Acids Res.*, **43**, e149.
14. Hernández,A.R. and Kool,E.T. (2011) The components of xRNA: Synthesis and fluorescence of a full genetic set of Size-Expanded ribonucleosides. *Org. Lett.*, **13**, 676–679.
15. Börjesson,K., Preus,S., El-Sagheer,A.H., Brown,T., Albinsson,B. and Wilhelmsson,L.M. (2009) Nucleic Acid base analog FRET-Pair facilitating detailed structural measurements in nucleic acid containing systems. *J. Am. Chem. Soc.*, **131**, 4288–4293.

16. Bood,M., Füchtbauer,A.F., Wranne,M.S., Ro,J.J., Sarangamath,S., El-Sagheer,A.H., Rupért,D.L.M., Fisher,R.S., Magennis,S.W., Jones,A.C. *et al.* (2018) Pentacyclic adenine: a versatile and exceptionally bright fluorescent DNA base analogue. *Chem. Sci.*, **9**, 3494–3502.
17. Han,J.H., Yamamoto,S., Park,S. and Sugiyama,H. (2017) Development of a Vivid FRET system based on a highly Emissive dG-dC Analogue pair. *Chem. Eur. J.*, **23**, 7607–7613.
18. Miller,M.L. and Doran,M. (1956) Concentrated Salt Solutions. II. Viscosity and density of sodium thiocyanate, sodium perchlorate and sodium iodide. *J. Phys. Chem.*, **60**, 186–189.
19. Preus,S., Kilså,K., Miannay,F.A., Albinsson,B. and Wilhelmsson,L.M. (2013) FRETmatrix: a general methodology for the simulation and analysis of FRET in nucleic acids. *Nucleic Acids Res.*, **41**, e18.
20. Lu,X.J. and Olson,W.K. (2003) 3DNA: a software package for the analysis, rebuilding and visualization of three-dimensional nucleic acid structures. *Nucleic Acids Res.*, **31**, 5108–5121.
21. Olson,W.K., Bansal,M., Burley,S.K., Dickerson,R.E., Gerstein,M., Harvey,S.C., Heinemann,U., Lu,X.J., Neidle,S., Shakked,Z. *et al.* (2001) A standard reference frame for the description of nucleic acid base-pair geometry. *J. Mol. Biol.*, **313**, 229–237.
22. Sandin,P., Börjesson,K., Li,H., Mårtensson,J., Brown,T., Wilhelmsson,L.M. and Albinsson,B. (2008) Characterization and use of an unprecedentedly bright and structurally non-perturbing fluorescent DNA base analogue. *Nucleic Acids Res.*, **36**, 157–167.
23. Preus,S., Börjesson,K., Kilså,K., Albinsson,B. and Wilhelmsson,L.M. (2010) Characterization of nucleobase analogue FRET acceptor tC_{nitro}. *J. Phys. Chem. B.*, **114**, 1050–1056.
24. Zheng,G.H., Lu,X.J. and Olson,W.K. (2009) Web 3DNA-a web server for the analysis, reconstruction, and visualization of three-dimensional nucleic-acid structures. *Nucleic Acids Res.*, **37**, W240–W246.
25. Serebryany,V. and Beigelman,L. (2002) An efficient preparation of protected ribonucleosides for phosphoramidite RNA synthesis. *Tetrahedron Lett.*, **43**, 1983–1985.
26. Sinha,N.D., Biernat,J., McManus,J. and Köster,H. (1984) Polymer support oligonucleotide synthesis XVIII: Use of β-Cyanoethyl-*N*,*N*-Dialkylamino-/*N*-Morpholino phosphoramidite of deoxynucleosides for the synthesis of DNA Fragments simplifying deprotection and isolation of the final product. *Nucleic Acids Res.*, **12**, 4539–4557.
27. Xu,Y., Ishizuka,T., Kimura,T. and Komiyama,M. (2010) A U-Tetrad stabilizes human telomeric RNA G-Quadruplex structure. *J. Am. Chem. Soc.*, **132**, 7231–7233.
28. Wang,A.H.J., Quigley,G.J., Kolpak,F.J., Crawford,J.L., Vanboom,J.H., Vandermarel,G. and Rich,A. (1979) Molecular structure of a Left-Handed double helical DNA fragment at atomic resolution. *Nature*, **282**, 680–686.
29. Hall,K., Cruz,P., Tinoco,I., Jovin,T.M. and Vandesande,J.H. (1984) Z-RNA - a Left-Handed RNA double helix. *Nature*, **311**, 584–586.
30. Zarling,D.A., Calhoun,C.J., Feuerstein,B.G. and Sena,E.P. (1990) Cytoplasmic microinjection of immunoglobulin Gs recognizing RNA helices inhibits human cell growth. *J. Mol. Biol.*, **211**, 147–160.
31. Placido,D., Brown,B.A., Lowenhaupt,K., Rich,A. and Athanasiadis,A. (2007) A left-handed RNA double helix bound by the Z alpha domain of the RNA-editing enzyme ADAR1. *Structure*, **15**, 395–404.
32. Popenda,M., Milecki,J. and Adamiak,R.W. (2004) High salt solution structure of a left-handed RNA double helix. *Nucleic Acids Res.*, **32**, 4044–4054.
33. Schwartz,T., Rould,M.A., Lowenhaupt,K., Herbert,A. and Rich,A. (1999) Crystal structure of the Z alpha domain of the human editing enzyme ADAR1 bound to left-handed Z-DNA. *Science*, **284**, 1841–1845.